**Frontiers in Computing and Intelligent Systems**
ISSN: 2832-6024 | Vol. 10, No. 1, 2024

# A Method of Dynamic Spatial Positioning of the Eyeball Based on Optic Disc Feature Following in Infants and Young Children

**Mingjun Ju [1], Zhongmin Li [2, *], Jing Wang [2], Xiaohui Guo [2], Biao Hu [1]**

[1] Engineering Laboratory for Safe and Precise Coal Mining of Anhui Province, School of Mechanical and Electrical Engineering, Anhui University of Science and Technology, Huainan, Anhui, China
[2] Department of Ophthalmology, Fuyang Women and Children's Hospital, Fuyang, Anhui, China
[*] **Corresponding author**: Zhongmin Li (Email: jmj18891468122@163.com)

**Abstract:** The dynamic spatial positioning of infants' eyes is crucial in ophthalmic retinal screening and medical imaging research. It plays an important role in the diagnosis of retinal diseases, the design of personalized treatment plans, and the monitoring of ophthalmic surgery. In order to solve the defects of existing eye tracking equipment and technology, such as complex implementation, sensitivity to environmental conditions, and limited long-term use, this study proposed a dynamic spatial positioning method of the eye based on the characteristics of the optic disc of infants. This method calibrates the size of the eye and retinal image through digital-analog linkage technology. It establishes a mapping relationship between pixels and physical sizes, and effectively solves the perspective distortion problem in retinal image acquisition, improving positioning accuracy and reliability. The centroid of the optic disc is selected as the reference point for spatial transformation, and the dynamic spatial changes of the eye are converted into changes in the centroid of the optic disc. Experimental results show that this method has good accuracy and robustness. The accuracy of dynamic spatial positioning of the eye is 0.0001 mm, and its average error is 0.000888 mm.

**Keywords:** Optic Papilla; Dynamic Spatial Positioning; Digital-analog Linkage; Visual Angle Distortion.

## 1. Introduction

In recent years, with the increasing social pressure people face, this has led to an increase in the number of older mothers and an increase in high-risk factors for infant development. The dynamic spatial positioning of the eyeball is of great significance in fundus screening and medical imaging research for infants and young children. In particular, its research is of great significance in the diagnosis of retinal diseases, the design of personalized treatment plans, and the monitoring of ophthalmic surgery.

In the early diagnosis and monitoring of ophthalmic diseases, dynamic spatial positioning of the eyeball can help doctors better understand the real-time position and movement direction of the eyeball. It can accurately diagnose and treat retinal diseases. Mainly reflected in the fact that before ophthalmic surgery, real-time acquisition of the eyeball position can provide doctors with important references and improve the safety and effectiveness of the surgery. At the same time, personalized treatment plans based on the spatial position and posture of the eyeball can improve the treatment effect. In terms of personalized treatment plan design, by accurately tracking the movement of the eyeball, it is possible to better formulate personalized treatment plans for patients [1, 2]. Especially in refractive surgery using laser means, accurate eye positioning can help doctors avoid damaging surrounding tissues during laser treatment [3, 4]. In ophthalmic scientific research, dynamic spatial positioning of the eyeball helps disciplines to deeply understand the relationship between eye movement and visual processing, and provide theoretical and data support for basic research.

Eye position tracking devices and rotation positioning methods have always attracted attention. Although many devices and methods have emerged, there are still some compromises [5-7]. In terms of eye spatial positioning technology, the search coil method uses a magnetic induction coil to detect the external applied magnetic field of the induction coil around the subject. The position of the eye is calculated based on the relative amplitude of the sensor output frequency [8]. However, this method is easily interfered by the environmental magnetic field, and the installation of the induction coil has high requirements for experimental design and is not suitable for long-term application. In 1997, Mulligan et al. proposed an eye tracking method based on retinal vascular images. The eye movement is accurately monitored by analyzing the changes in the vascular pattern on the retina. This method has higher optical gain and robustness [9]. However, this method relies on high-resolution image acquisition and may be affected by factors such as image blur or optical distortion. In addition, slit lamp pre-mirror examination, Fison observation and fundus photography can also be used to measure the disc-fovea angle (DFA) to objectively judge the state of eye rotation [1, 2, 10-12]. However, this method is highly instrument-dependent and has limited application scenarios. Pupil center corneal reflection (PCCR) uses a near-infrared camera to capture eye movements using a light source that illuminates the eye and causes visible reflections. The vector formed by the angle between the corneal and pupil reflections is calculated to reflect the rotation angle of the eye. However, the accuracy of corneal reflection is easily affected by light conditions and reflection interference. In 2004, researchers at the School of Medicine comprehensively explored the potential and application prospects of combining eye tracking technology with machine learning and deep learning algorithms. The fusion of this method not only optimized the accuracy of data annotation and enhanced the accuracy of image classification, but also made significant improvements in pathology detection and segmentation tasks. The research on eye tracking combined with artificial intelligence has opened up new possibilities for improving the efficiency and accuracy of medical image analysis [13]. However, data collection requires high-precision equipment and strict experimental conditions, which limits the convenience and scalability of data collection. Research focuses on two-dimensional images. How to use this data to enhance three-dimensional models remains an underexplored area. Secondly, the interpretability and generalization capabilities of the model are not strong.

In the research of eye position tracking equipment, the VisxS$^4$IK excimer laser machine can not only automatically track the horizontal X and Y axis displacement of the eyeball and the vertical Z axis displacement, but also measure the angle of eyeball rotation and the distance of pupil center displacement, and provide prompts and compensation. From the original XYZ three-dimensional tracking, it has been expanded to three-dimensional tracking plus eyeball rotation positioning [14]. Synoptophores measure the conscious and perceived tilt angles, as well as detect subjective rotation degrees and binocular vision function [15, 16]. The Bagolini linear mirror test determines the visual state by evaluating retinal correspondence [17]. Using the iris camera of the laser machine to collect images during surgery to calculate the rotation angle of the eyeball and the displacement of the pupil center is also widely used [18]. These devices are limited by high complexity. They are also limited by their dependence on specific operating environments and limited dynamic tracking capabilities. The breadth and flexibility of device applications are very poor.

In this paper, we proposed a method for dynamic spatial positioning of the eyeball based on the characteristics of the optic disc of infants and young children. We firstly modeled the eyeball and calibrated the size of the fundus image based on the digital-analog linkage technology, so that the pixel-size relationship between the spatial eyeball and the two-dimensional image was established. Then, we fully considered the influence of the perspective distortion of the sphere in image acquisition and proposed a positioning scheme for the centroid feature of the optic disc. We selected the centroid of the optic disc as the target point for spatial transformation recognition. Finally, the dynamic spatial transformation of the eyeball was converted into the spatial transformation of the centroid of the optic disc, and its effectiveness was analyzed. Experiments have shown that this method is a universal method for dynamic spatial positioning of the eyeball. This model and method can be used for dynamic spatial positioning of the eyeball in common fundus examinations that obtain the optic disc. It has high detection accuracy, strong robustness, and high flexibility, and is fully suitable for clinical research and scientific research on spatial positioning of the eyeball in auxiliary ophthalmology.

# 2. Dynamic Spatial Positioning of the Eyeball

We propose a dynamic spatial positioning method for the eyeball based on the characteristics of the infant optic disc. The main target population is infants aged 0 to 12 years old, and the fundus screening device used is RetCam Ⅲ. It will be equipped with a D1300 lens. An examiner will take at least 10 images. A total of 200 original images were collected to construct the dataset. The image resolution is 1600×1200. The images are saved in PNG format.

## 2.1. Preparation

Before elaborating on the method of dynamic spatial positioning of the eyeball, the basic size data of the eyeball and the calibration of the fundus image size will be the first preparatory work to be completed. First, the basic size data of the eyeball provides the calculation basis for the mathematical method of spatial positioning. Fundus image size calibration establishes the correspondence between image pixel information and actual eyeball space physical information. Secondly, the combination of the basic size data of the eyeball and the fundus image size calibration enables the system to accurately convert the observation points on the image into accurate physical positions, thereby realizing accurate tracking and analysis of eyeball movements.

In recent years, most ophthalmic clinical trials and scientific research cannot accurately provide the size parameters of the invisible internal structures of the eyeball [19]. This study reviewed a large number of studies on the structural parameters of infants and young children's eyes, especially the fundus size data that can be imaged by the RetCam Ⅲ device for infants and young children. The researchers used the default assumption of an axial length of 24 mm to calculate the area [20]. The researchers used an axial length of 24 mm to represent the optical model of the Navarro UWF model eye. This is to enable experimenters to more accurately calculate the anatomically correct area of the vascularized retina when performing stereoscopic projection and image stitching [21]. The study expressed the relationship between axial length and age, gender, height, and body mass index (BMI). The standard value of axial length is generally considered to be 24 mm, regardless of gender, race, and other physical parameters [22]. In summary, the fundus of the eyeball is defined as a hemisphere with a diameter of 24 mm.

Fundus image size calibration uses a multi-point calibration method, using the sizes of multiple known targets for calibration. In 2006, De Silva et al. evaluated the optic disk size and the distance from the optic disk to the macula of premature and full-term infants. The study found that the average value of the optic disk height (ODH) was $1.41 \pm 0.19$ mm; the average value of the optic disk width (ODW) was $1.05 \pm 0.13$ mm; the average value of the optic disk-to-fovea distance (ODF) was $4.4 \pm 0.4$ mm; and the optic disk diameter (ODD) [23]. Using this study as a reference, the optic disk height, optic disk width, and optic disk-to-fovea distance in the image were used as known sizes for joint calibration. As shown in Figure 1, the experiment recorded their pixel positions in the image and calculated the ratio between the actual size of each object and the pixel size. Through regression analysis method, a more accurate scaling factor is obtained and applied to the whole image.

Since the eyeball is a sphere, the fundus will inevitably have the problem of perspective distortion during the shooting process. The closer the fundus information is to the edge of the camera's perspective, the more information will be compressed and missing. In response to this dilemma, new requirements are brought to the calibration of fundus image size. We have established a feedback system for the calibration of known areas. As shown in Figure 1, we assume that the fundus is the northern hemisphere of the earth. According to the study of Universal Polar Stereographic, the setting of the scale factor of 0.994 for areas above 80° north latitude is based on the comprehensive consideration of multiple factors such as geometric deformation, linear distortion and angle fidelity during polar map projection to reduce the distortion in the polar region. We believe that the projection information within 80° north latitude to 90° north latitude is about 0.6% smaller than the actual information. The distortion it contains can be ignored. In summary, the calibration feedback system we established is designed as follows: First, the image is calibrated using the multi-point calibration method, and the calculated scale factor is applied to the entire image. Secondly, take the center of the image as the origin and $r$ as the radius of the eyeball, and draw a circular surface at 80° north latitude in the image according to formula (1). Finally, ensure that the calibration of the known target in the multi-point calibration method is within the circular surface at 80° north latitude, then the calibration is considered qualified. Otherwise, this image will not be calibrated.

$$\begin{cases} z_{80°N} = r \cdot \cos(80°) \\ x^2 + y^2 = r^2 - z_{80°N}^2 \end{cases}. \tag{1}$$

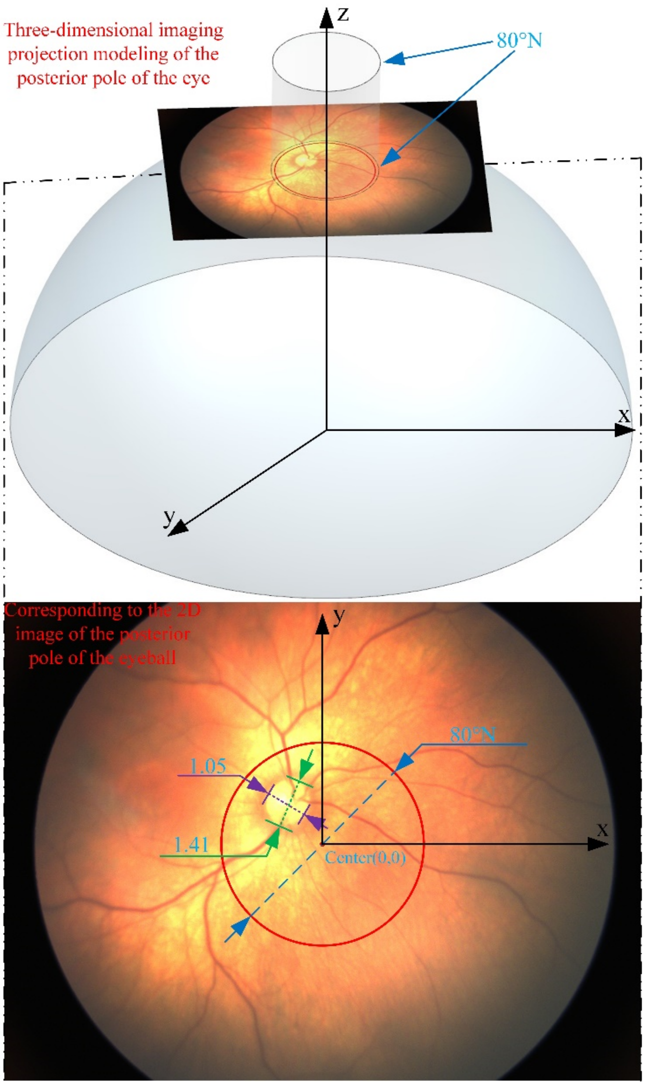


**Figure 1.** Image size calibration and perspective distortion display

## 2.2. Scheme for Optic Disc Feature Selection

The core of the eyeball dynamic spatial positioning method is to analyze the changes in the optic disc of the fundus to accurately monitor the movement of the eyeball. Therefore, the selection of optic disc features is the most important part of the detection target. The prominence and recognition accuracy of the features directly determine the accuracy of the positioning method.

### 2.2.1. Optic Disc Center

As a key component of the infant eye structure, the optic disc plays a vital role in the screening of infant eye diseases. A comprehensive examination is an indispensable step [24]. At the same time, we found that almost all eye screening images contain the optic disc and macula. Therefore, we chose the optic disc as the target feature for the dynamic spatial positioning of the eyeball.

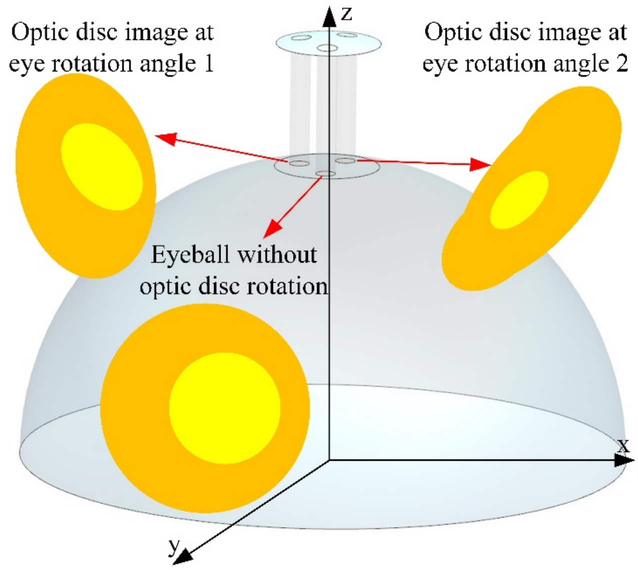


**Figure 2.** Orthogonal projection of the optic disc at different rotation angles

As shown in Figure 2, we are limited by the problem of perspective distortion during the fundus photography. It is very unscientific to directly track and identify the entire optic disc. Under the premise that the camera remains unchanged, the position of the optic disc in the acquired fundus image changes with the rotation of the eyeball. What is more fatal is that the size and shape of the optic disc are constantly changing. Therefore, we changed our thinking and proposed to locate the center of the optic disc. The spatial transformation of the eyeball is represented by the spatial transformation of the center of the optic disc.

Among the many concepts of two-dimensional centers such as centre of gravity, centroid, centre of mass, geometrical center, mean center, etc., we need to consider the ability of the center concept to handle irregular shape centers and resist perspective distortion. The optic disc centroid can better capture the characteristics of irregular shapes and provide a more realistic center position. Secondly, the calculation of the optic disc centroid is based on the information of all points. Compared with relying only on certain boundaries or vertices, the centroid can more comprehensively reflect the actual distribution of the object. Finally, the calculation of the optic disc centroid is simple and efficient. Finally, we choose the optic disc centroid as the target point for spatial transformation recognition. A more detailed argument will be developed in 3.1.

### 2.2.2. Calibration of the Centroid of the Optic Papilla

According to the theory in 2.2.1, we have solved the distortion problem that affects the location of the optic disc center. To locate the optic disc center, we only need to calculate the centroid of the optic disc at each angle. The method design is shown in Figure 3.

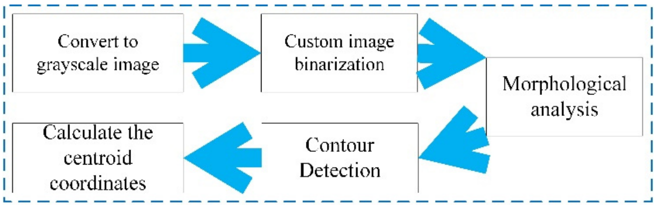


**Figure 3.** Calibration design of the optic papillary centroid

We take the center pixel of the image as the origin (0, 0) and use pixels as coordinate units to establish a two-dimensional coordinate system. The x-axis is positive to the right and the y-axis is positive upward. First, convert the fundus color image into a grayscale image according to formula (2). *R* is the value of the red channel, *G* is the value of the green channel, *B* is the value of the blue channel, and *Gray* is the calculated grayscale value.

$$\mathrm{Gray} = 0.2989 \times R + 0.5870 \times G + 0.1140 \times B. \quad (2)$$

Then, the grayscale image is converted into a binary image according to formula (3).

$$\mathrm{Binary}(x,y) = \begin{cases} 255 & \mathrm{ifGray}(x,y) \geq T \\ 0 & \mathrm{ifGray}(x,y) < T \end{cases}. \quad (3)$$

Among them, *Gray*(x,y) is the pixel value of the grayscale image at the coordinate (x,y), *T* is set to 200, and *Binary*(x,y) is the pixel value of the binary image at the coordinate (x,y).

According to formula (4), the pixel values in the image are operated according to their shape or structure. Create a 5 * 5 rectangular structure element. Use erosion to remove small protrusions in the image.

$$E(x,y) = \min_{(x',y') \in B} I(x+x', y+y'). \quad (4)$$

Where *I*(x,y) is the pixel value of the original image at (x,y), *B* is the structural element, and *E*(x,y) is the pixel value of the eroded image at (x,y).

Dilation can restore the edge of the object removed during the erosion process. According to formula (5), for each pixel point *P*(x,y) in the image, it is compared with the structural element *B*. If the structural element *B* has any overlap with the foreground pixel at *P*(x,y), that is, *B* covers any foreground pixel of *I*(x,y), then *P*(x,y) is set to the foreground value; otherwise, keep its original value or set it to the background value.

$$D(x,y) = \max_{(x',y') \in B} I(x+x', y+y'). \quad (5)$$

Where *D*(x,y) is the pixel value at (x,y) in the dilated image.

Combining erosion and dilation, the opening operation is shown in Equation (6), which removes small white noise points while maintaining the integrity of larger objects. When processing fundus images, this helps to clearly identify important structures such as the optic disc.

$$\begin{cases} O(x,y) = \mathrm{Dilation}(\mathrm{Erosion}(I(x,y),B),B) \\ O(x,y) = \max_{(x',y') \in B} \min_{(x'',y'') \in B} I(x+x'-x'', y+y'-y'') \end{cases} \quad (6)$$

Where *O*(x,y) is the pixel value of the image at (x,y) after the opening operation.

Contour detection uses the Douglas-Peucker algorithm to start from the starting point of the contour, find the farthest point, and create a line segment connecting the two points. Next, the algorithm checks each point on the contour to see if they are near this line segment. The distance calculation formula is shown in equation (7). If not, these points will be retained, and the algorithm will repeat this process on these points until all points have been checked.

$$d(P, line) = \min_{x \in line} \sqrt{(x-P_x)^2 + (y-P_y)^2}. \quad (7)$$

Among them, *P*(x,y) is the point on the contour, line is the current line segment, and $(P_x,P_y)$ is the coordinate of point *P*.

According to the description in 2.2.1 above, the centroid of the optic disc contour is calculated according to formula (8), and we have completed the calibration of the centroid of the optic disc.

$$x_c = \frac{\sum_{i=1}^{N} x_i}{N}, y_c = \frac{\sum_{i=1}^{N} y_i}{N}. \quad (8)$$

## 2.3. Establishment of a Dynamic Spatial System of Optic Disc Features

The eyeball space coordinate system is established with the eyeball center (0, 0, 0) as the sphere center, a radius of 12mm, and millimeters as the coordinate unit. We will expand the two-dimensional plane coordinate system established in 2.2.2 to the three-dimensional space coordinate system calculation. Because the eyeball center (0, 0, 0) is the sphere center in the three-dimensional coordinate system, and the two-dimensional plane coordinate system is established with the image center as the origin in 2.2.2, the relationship between the two coordinate systems is shown in the figure. The coordinates of any optic disc centroid $(x_1, y_1)$ in the original two-dimensional coordinate system are converted to $(x_1, y_1, \sqrt{12^2 - {x_1}^2 - {y_1}^2})$ in the three-dimensional coordinate system. For the convenience of calculation, we define any optic disc centroid point as $(x_1, y_1, z_1)$. Assume that the center of the fundus of the standard eyeball, that is, the center point of the optic disc, is (0, 0, 12) (hereinafter collectively referred to as the standard point). For the convenience of calculation, we define the standard point as (x, y, z). In three-dimensional space, the rotation matrix is shown in equations (9), (10), and (11).

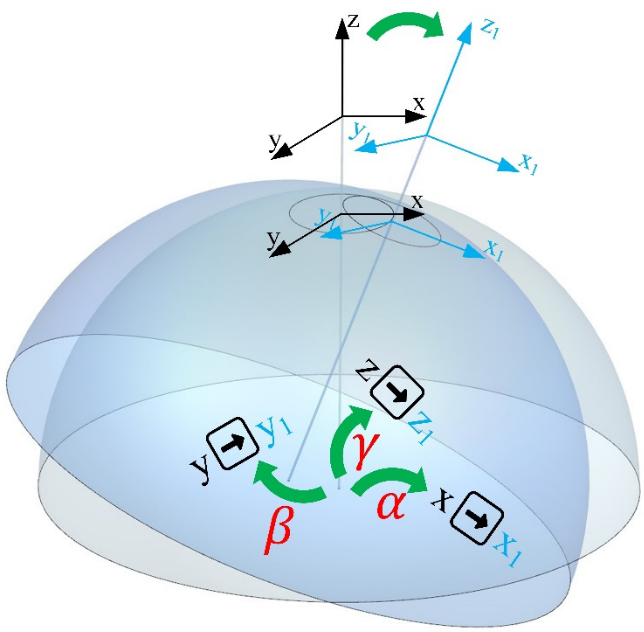


**Figure 4.** Schematic diagram of eyeball dynamic rotation

The matrix for rotating $\alpha$ around the x-axis:

$$R_x(\alpha) = \begin{bmatrix} 1 & 0 & 0 \\ 0 & \cos(\alpha) & -\sin(\alpha) \\ 0 & \sin(\alpha) & \cos(\alpha) \end{bmatrix}. \quad (9)$$

The matrix for rotating $\beta$ around the y-axis:

$$R_y(\beta) = \begin{bmatrix} \cos(\beta) & 0 & \sin(\beta) \\ 0 & 1 & 0 \\ -\sin(\beta) & 0 & \cos(\beta) \end{bmatrix}. \quad (10)$$

The matrix for rotating $\gamma$ around the z-axis:

$$R_z(\gamma) = \begin{bmatrix} \cos(\gamma) & -\sin(\gamma) & 0 \\ \sin(\gamma) & \cos(\gamma) & 0 \\ 0 & 0 & 1 \end{bmatrix}. \quad (11)$$

The transformed position is known:

$$\begin{bmatrix} x_1 \\ y_1 \\ z_1 \end{bmatrix} = R_z(\gamma) R_y(\beta) R_x(\alpha) \cdot \begin{bmatrix} x \\ y \\ z \end{bmatrix}. \quad (12)$$

The rotation angles $\alpha$, $\beta$, and $\gamma$ are efficiently calculated from the inverse transformation.

$$\begin{cases} \sin(\beta) = \frac{z_1}{\sqrt{x_1^2+y_1^2+z_1^2}} \\ \cos(\gamma) = \frac{x_1\cos(\beta)+y_1\sin(\beta)}{x} \\ \sin(\gamma) = -\frac{y_1\cos(\beta)-x_1\sin(\beta)}{x} \\ \sin(\alpha) = \frac{y_1\cos(\beta)-z_1\sin(\beta)}{x} \\ \cos(\alpha) = \frac{y_1\sin(\beta)+z_1\cos(\beta)}{x} \end{cases}. \quad (13)$$

Eye rotation is defined as positive in the clockwise direction and negative in the counterclockwise direction around the x, y, and z axes.

# 3. Experiment and Analysis

The experimental demonstration and analysis are mainly divided into two parts. The demonstration of the centroid mainly proves the accuracy of the optic disc centroid as the target point for spatial transformation identification through simulation experiments. The experimental demonstration mainly measures the accuracy and error of the eye dynamic spatial positioning method of optic disc feature following through eye rotation simulation experiments to prove the effectiveness of this method.

## 3.1. Centroid Argument

We will discuss four concepts of center, namely center of gravity, centroid, center of mass and geometric center. Three plane figures are simulated to simulate the optic disc of the fundus, namely circle, ellipse and custom-designed irregular ellipse. According to the research limitations of Universal Polar Stereographic, the eye rotation angles are set to 2.5°, 5° and 7.5° around the z-axis respectively. According to the optic disc characteristic dynamic space system established in 2.3 above, it is easy to calculate the coordinates of the center point of the optic disc after rotation, which are (0.523428, 0.000000, 11.988581) (1.045869, 0.000000, 11.954336) (1.566314, 0.000000, 11.897338) given the coordinates of the standard point of the optic disc.

After the standard optic disc center point after eye rotation is known, the optic disc after eye rotation in this coordinate system is vertically projected onto the plane of z=0. According to the optic disc feature selection method in 2.2 above, the two-dimensional coordinate points of the center of gravity, centroid, center of mass and geometric center of the optic disc after actual eye rotation are calculated. The two-dimensional coordinates are expanded to three-dimensional spatial coordinates according to the eye model. The three-dimensional spatial coordinates of the actual centers are obtained and compared with the standard optic disc center point. The three graphics at different angles were subjected to 10 simulated rotation experiments. The average data of the experiments at the same angle are shown in Figure 5. The average error of the centroid is 0.001984mm, the average error of the center of gravity is 0.001994mm, the average error of the center of mass is 0.001988mm, and the average error of the geometric center is 0.002000mm. We can see that the centroid is the central conceptual point closest to the standard optic disc center.

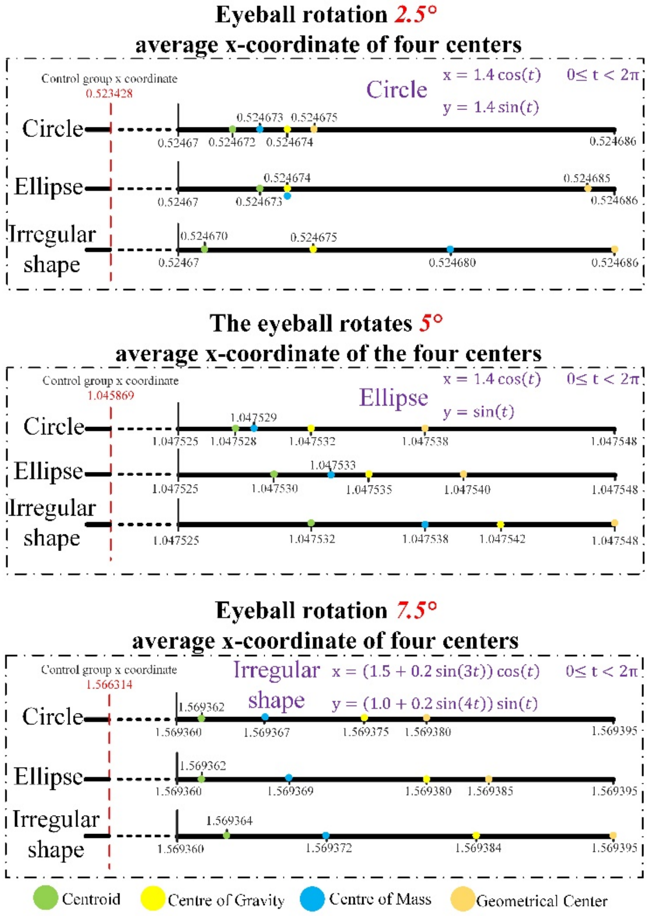


**Figure 5.** Average x-coordinate value at different rotation angles and different centers

## 3.2. Experimental Design

In actual clinical eye screening, we are limited by medical conditions, ethical principles, laws and regulations. We cannot actually demonstrate the accuracy of the dynamic spatial positioning method of the eyeball based on the characteristics of the optic disc of infants and young children. Based on the centroid demonstration in 3.1, the accuracy and error of the dynamic spatial positioning method of the eyeball based on the characteristics of the optic disc are measured through an eye rotation simulation experiment.

Assume that we know the coordinates of the standard point and the coordinates of the centroid of the optic disc after rotation around the z-axis $\theta_1$, $\theta_2$, and $\theta_3$, that is, (0.523428, 0.000000, 11.988581) (1.045869, 0.000000, 11.954336) (1.566314, 0.000000, 11.897338). Inversely calculate $\theta_1$, $\theta_2$, and $\theta_3$ rotated around the z-axis. The calculated results are 2.51°, 4.99° and 7.49° respectively, with an accuracy of 0.0001mm and an average error of 0.000888mm.

# 4. Conclusion

This paper introduces a method for dynamic spatial positioning of the eyeball based on the characteristics of the optic disc of infants and young children. By modeling the eyeball and calibrating the size of the fundus image based on the digital-analog linkage technology, a pixel-size relationship is established between the spatial eyeball and the two-dimensional image. Taking into full consideration the influence of the perspective distortion of the sphere in image acquisition, a positioning scheme for the centroid features of the optic disc is proposed based on a comprehensive analysis of multiple factors such as the geometric deformation, linear distortion and angle fidelity of Universal Polar Stereographic to improve positioning accuracy and reduce distortion. The dynamic spatial transformation of the eyeball is converted into the spatial transformation of the centroid of the optic disc, and its effectiveness is analyzed. Experiments have shown that this method is a universal method for dynamic spatial positioning of the eyeball. This model and method can be used for dynamic spatial positioning of the eyeball in common fundus examinations that obtain the optic disc. The accuracy is 0.0001mm and the average error is 0.000888mm. This method provides a generalizable solution for dynamic spatial positioning in clinical and research ophthalmology, and has great potential to improve the safety and effectiveness of ophthalmic surgery and personalized treatment.

# Acknowledgments

This work was supported in part by a grant from Engineering Laboratory for Safe and Precise Coal Mining of Anhui Province Open Fund Project (ESCMP202406), Health research project of Anhui Province (AHWJ2023A30243).

# References

[1] G Helveston E M, Krach D, Plager D A, et al. A new classification of superior oblique palsy based on congenital variations in the tendon[J]. Ophthalmology, 1992, 99(10): 1609-1615.

[2] Straumann D, Steffen H, Landau K, et al. Primary position and Listing's law in acquired and congenital trochlear nerve palsy[J]. Investigative ophthalmology & visual science, 2003, 44(10): 4282-4292.

[3] Swami A U, Steinert R F, Osborne W E, et al. Rotational malposition during laser in situ keratomileusis[J]. American journal of ophthalmology, 2002, 133(4): 561-562.

[4] Chernyak D A. Cyclotorsional eye motion occurring between wavefront measurement and refractive surgery[J]. Journal of Cataract & Refractive Surgery, 2004, 30(3): 633-638.

[5] Müller P U, Cavegn D, d'Ydewalle G, et al. A comparison of a new limbus tracker, corneal reflection technique, Purkinje eye tracking and electro-oculography[J]. 1993.

[6] Ydewalle G, Rensbergen J V. Perception and cognition: Advances in eye movement research[J]. (No Title), 1993.

[7] Young L R, Sheena D. Survey of eye movement recording methods[J]. Behavior research methods & instrumentation, 1975, 7(5): 397-429.

[8] Robinson D A. A method of measuring eye movemnent using a scieral search coil in a magnetic field[J]. IEEE Transactions on bio-medical electronics, 1963, 10(4): 137-145.

[9] Mulligan J B. Image processing for improved eye-tracking accuracy[J]. Behavior Research Methods, Instruments, & Computers, 1997, 29(1): 54-65.

[10] Straumann D, Steffen H, Landau K, et al. Primary position and Listing's law in acquired and congenital trochlear nerve palsy[J]. Investigative ophthalmology & visual science, 2003, 44(10): 4282-4292.

[11] Clark R A, Miller J M, Demer J L. Displacement of the medial rectus pulley in superior oblique palsy[J]. Investigative ophthalmology & visual science, 1998, 39(1): 207-212.

[12] Oh S Y, Clark R A, Velez F, et al. Incomitant strabismus associated with instability of rectus pulleys[J]. Investigative ophthalmology & visual science, 2002, 43(7): 2169-2178.

[13] Moradizeyveh S, Tabassum M, Liu S, et al. When Eye-Tracking Meets Machine Learning: A Systematic Review on Applications in Medical Image Analysis[J]. arXiv preprint arXiv:2403.07834, 2024.

[14] Chernyak D A. From wavefront device to laser: an alignment method for complete registration of the ablation to the cornea [J]. Journal of Refractive Surgery, 2005, 21(5).

[15] Clemons T E, Rankin M W, McBee W L. Cognitive impairment in the age-related eye disease study: AREDS report no. 16[J]. Archives of Ophthalmology (Chicago, Ill.: 1960), 2006, 124(4): 537-543.

[16] Thomas S L, Thomas S D M. Displacement and health[J]. British medical bulletin, 2004, 69(1): 115-127.

[17] von Hanno T, Lade A C, Mathiesen E B, et al. Macular thickness in healthy eyes of adults (N= 4508) and relation to sex, age and refraction: the Tromsø Eye Study (2007–2008)[J]. Acta ophthalmologica, 2017, 95(3): 262-269.

[18] Lie J T, Birbal R, Ham L, et al. Donor tissue preparation for Descemet membrane endothelial keratoplasty[J]. Journal of Cataract & Refractive Surgery, 2008, 34(9): 1578-1583.

[19] Boote C, Sigal I A, Grytz R, et al. Scleral structure and biomechanics[J]. Progress in retinal and eye research, 2020, 74: 100773.

[20] Tan C S, Chew M C, van Hemert J, et al. Measuring the precise area of peripheral retinal non-perfusion using ultra-widefield imaging and its correlation with the ischaemic index[J]. British Journal of Ophthalmology, 2016, 100(2): 235-239.

[21] Singer M, Sagong M, van Hemert J, et al. Ultra-widefield imaging of the peripheral retinal vasculature in normal subjects[J]. Ophthalmology, 2016, 123(5): 1053-1059.

[22] Palchunova K, Mino T, Mihashi T, et al. Precise retinal shape measurement by alignment error and eye model calibration[J]. Optical Review, 2022, 29(3): 188-196.

[23] De Silva D J, Cocker K D, Lau G, et al. Optic disk size and optic disk-to-fovea distance in preterm and full-term infants[J]. Investigative ophthalmology & visual science, 2006, 47(11): 4683-4686.

[24] Sabri K, Ells A L, Lee E Y, et al. Retinopathy of prematurity: a global perspective and recent developments[J]. Pediatrics, 2022, 150(3).